

Autonomous Suturing Via Surgical Robot: An Algorithm for Optimal Selection of Needle Diameter, Shape, and Path*

Sahba Aghajani Pedram¹, Peter Ferguson¹, Ji Ma¹, Erik Dutson², and Jacob Rosen¹

Abstract—In autonomous suturing with a surgical robot, needle shape, diameter, and path are critical parameters that directly affect suture depth and tissue trauma. This paper presents an optimization-based approach to specify these parameters. Given clinical suturing guidelines, a kinematic model of needle-tissue interaction was developed to quantify suture parameters and constraints. The model was further used to formulate constant curvature needle path planning as a nonlinear optimization problem. The inputs of the optimization include the tissue geometry, surgeon defined entry/exit points, and optimization weighting factors. The outputs are the needle geometry and suggested path. Off-line simulations were used to evaluate the accuracy and performance of the proposed model, and to determine optimized needle geometry and path for several clinically relevant input sets. The output and the optimization results were confirmed experimentally with the Raven II surgical system. The proposed needle path planning algorithm guarantees minimal tissue trauma and complies with a wide range of suturing requirements.

I. INTRODUCTION

A surgical procedure may be decomposed into subtasks including dissection, suturing, and tissue manipulation. Suturing is one of the most challenging and time consuming of all surgical subtasks [1]. In minimally invasive surgery (MIS), deficiencies such as reduced surgeon dexterity or limited visual feedback make this task even more challenging. Surgical robotic systems, such as the Raven II (see Fig. 1), have solved many of these deficiencies by providing additional degrees of freedom and leveraging sophisticated vision systems [2], [3], [4]. However, suturing with these systems, in which the surgeon serves as both the decision maker and the operator, is still difficult. For example, it is challenging for the surgeon to estimate distances and angles through an endoscope. Additionally, with limited vision and/or haptic feedback, extracting the needle from the desired point often requires multiple attempts, resulting in increased tissue trauma and extended operation time [5]. The limitations associated with the human operator along with the repetitive nature of suturing make it a candidate subtask for automation. The framework of automating suturing relies on

*This work is supported by the U.S. National Science Foundation award IIS-1227184: Multilateral Manipulation by Human-Robot.

¹Sahba Aghajani Pedram, Peter Ferguson, Ji Ma, and Jacob Rosen are with the Mechanical and Aerospace Engineering Department, University of California at Los Angeles, Los Angeles, CA, USA sahabaap@ucla.edu, pwferguson@ucla.edu, jima@ucla.edu jacobrosen@ucla.edu

²Erik Dutson is with the Department of Surgery, David Geffen School of Medicine, University of California at Los Angeles, Los Angeles, CA 90095, USA EDutson@mednet.ucla.edu

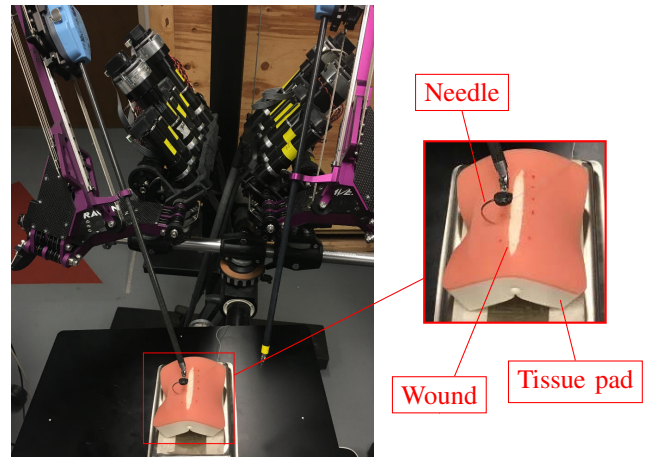
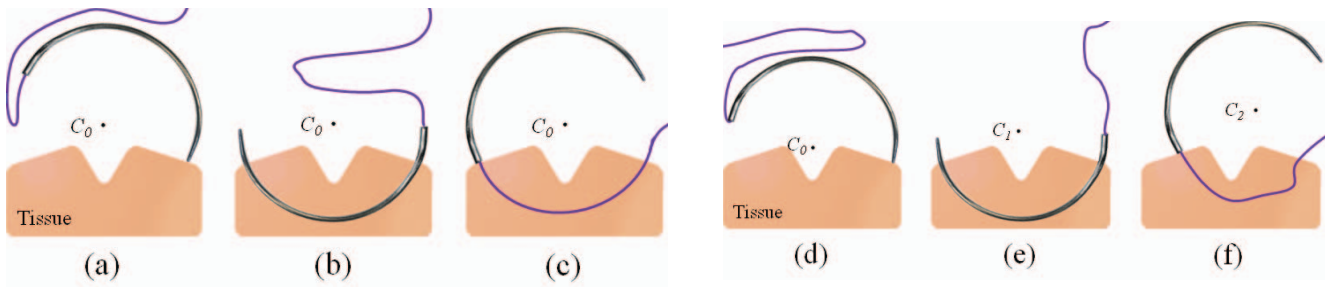


Fig. 1: Raven II autonomous suturing workstation.

the surgeon for high level decision making while delegating the execution of low-level motions to the robot, potentially leading to improved surgical outcome.

Previous studies have focused on different parts of fully automated suturing including knot tying [6], [7], [8], thread tracking [9], [10], and dexterous needle manipulation [11], [12], [13]. In particular, many research efforts focused on generating an initial needle path which can be updated in real time to adjust to environment changes. In [14], needle path planning has been formulated as a non-convex optimization problem subjected to kinematic constraints. This algorithm is designed to minimize the suture length and maintain orthogonal needle angle at the tissue entry point. Some studies [15], [16] have proposed constant curvature path (CCP) planning in which the needle only rotates around its geometric center to pierce the tissue (see Fig. 2a-Fig. 2c). It was argued in these studies that the CCP algorithm will result in minimal tissue trauma. However, due to the constrained motion, important suturing requirements such as adequate suture depth may not be satisfied [17], [18]. Needle reorientation inside the tissue is proposed in other studies [11], [14], [19], [20], [21], [22] to better follow suturing requirements yet it may impose tissue trauma [13].

Contribution: Despite the fact that surgeons select needle shape and diameter based on the wound/tissue geometry [23], [24], previous studies have largely ignored these variables in their path planning formulations. This study extends the current research effort by developing an algorithm that includes tissue/wound geometry as inputs, and needle shape/diameter



Fixed-center motion paradigm for needle path planning. (a) bite time, (b) switching time, (c) extraction time.

Moving-center motion paradigm for needle path planning. (d) bite time, (e) switching time, (f) extraction time.

Fig. 2: Fixed-center motion and moving-center motion concepts for needle path planning.

as outputs. Additionally, quantifying and minimizing error of various suture parameters is used to overcome CCP motion constraints and to fulfill a wide range of clinical suturing requirements. For accomplishing this goal, a kinematic model to describe the needle-tissue geometric relation and a nonlinear optimization formulation of the suture path are proposed. The resulting algorithm was tested experimentally using the Raven II surgical system.

II. METHOD

A. Suturing Guidelines

Suturing automation is based on clinical guidelines [19], [25] that can be summarized as follows:

Suture entry/exit angle: The needle should enter/exit the tissue orthogonally to minimize the shear stress around the entry/exit points.

Suture stitching: The needle should maneuver inside the tissue with minimal wrench to reduce tissue trauma.

Bite/Extraction: In the instant just before entering the tissue, called *bite time (BT)*, the rear end of the needle should not be in contact with the tissue. Similarly, in the instant just before the needle is extracted from the tissue, called *extraction time (ET)*, the tip should not touch the tissue.

Needle grasp: As the needle tip exits the tissue, there should be an instant, referred to as *switching time (ST)*, when both sides of the needle are able to be gripped. More specifically, the lengths of the needle outside of the tissue are equal on both sides.

Suture entry/exit points: The needle should enter/exit the tissue from points defined by the surgeon.

Suture depth: It is usually suggested that the ideal suture depth is equal to half the distance between the needle entry and exit points.

Suture symmetry: The suture should be symmetric about the wound to avoid uneven load distribution and trauma.

B. Needle Motion

Needle motion can be divided into two complementary categories: motion in which the needle center is fixed (see Fig. 2a-Fig. 2c) and motion in which the needle center is moving (see Fig. 2d-Fig. 2f).

In the first category, referred to as *Fixed-Center Motion (FCM)*, the needle only rotates around its stationary geometric center (e.g. C_0 in Fig. 2a-Fig. 2c). Note that the axis of rotation is orthogonal to the plane occupied by the needle. The second category, referred to as *Moving-Center Motion (MCM)*, includes all other motions. Namely, the needle can translate or rotate in any way that causes its geometric center to change position (e.g. C_0 , C_1 , and C_2 in Fig. 2d-Fig. 2f).

The needle path can be generated by FCM and/or MCM. The current study is focused only on FCM for two reasons. First, there is a general consensus in the medical community that following the natural curvature of the needle produces the best suture [5]. Second, as suggested by [13], although needle reorientation is possible in thin tissues, reorientation from MCM may cause thick tissue to tear.

On the other hand, the limitation of FCM is that any two combinations of suture parameters (defined below) will uniquely define the path. Due to this limitation, previous CCP planning algorithms only fulfilled a few suturing guidelines. For example, the method adopted in [15] met the entry and exit point criteria while the algorithm used in [16] accounted for entry point and entry angle requirements. Rather than satisfying a few suturing requirements, we bypass the limitation of FCM by permitting, weighting, and minimizing error for all suture parameters.

C. Kinematic Modeling of the Fixed-Center Motion Path

Assumptions: Similar to studies such as [16], [20], it is assumed that the forces/torques from needle-tissue interaction are negligible because FCM ideally creates small shear forces only. Under this assumption, neither the needle nor tissue deform significantly, and the suture path will be the same as the needle path. Hence, the needle path planning can be formulated as a kinematics problem. The needle is restricted to planar motion as implied by ideal FCM. The tissue geometry is assumed to be symmetric and is approximable by Fig. 3. It is assumed that the surgeon specifies symmetric desired entry and exit points on the tissue (I_d and O_d). Lastly, access to needle shapes $\in A_n = \{\frac{1}{4}, \frac{3}{8}, \frac{1}{2}, \frac{5}{8}\}$ is assumed.

Definitions and Conventions: The needle diameter refers to twice the distance from the geometric center of the needle to the tip. The needle shape refers to the arc length of the

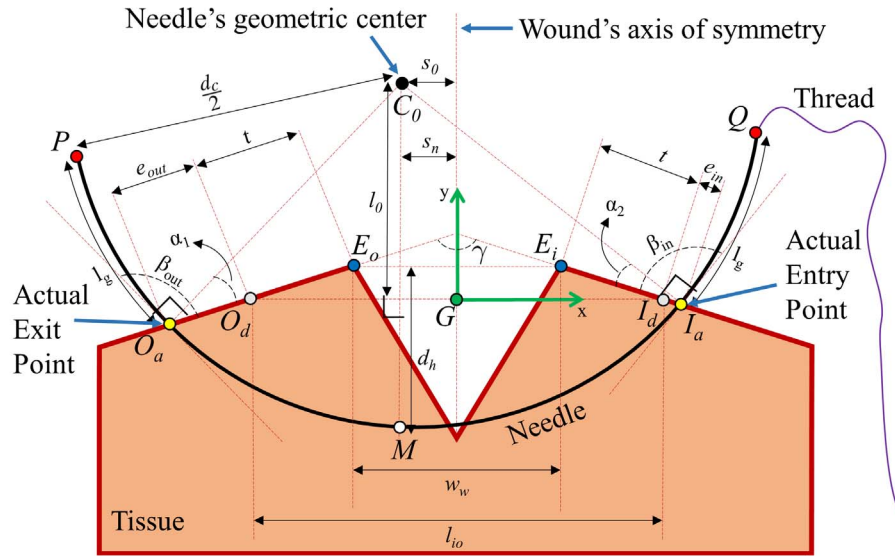


Fig. 3: Kinematic model of needle-tissue interaction at switching time.

needle as a fraction of the circumference of a circle. The needle path refers to the collection of needle tip configurations at each time step. These configurations are uniquely defined, in 2D, by the position of the needle center and needle diameter (the needle is assumed to rotate clockwise throughout the paper). All variables in the paper are listed in Table I.

We use, \vec{A} , to refer to vector A . The x and y components of \vec{A} are referred to as \vec{A}_x and \vec{A}_y . The unit vector from point A to point B is labeled $\hat{A}B$.

Suture Parameters: Based on the suturing guidelines, we define six *suture parameters* (shown in Fig. 3) that quantify an ideal needle path. These parameters are: 1) needle entry angle (β_{in}), 2) distance between actual and desired needle entry points (e_{in}), 3) needle depth (d_h), 4) needle-wound symmetry (s_n), 5) needle exit angle (β_{out}), and 6) distance between actual and desired needle exit points (e_{out}).

Needle Variables: Each suture parameters is a function of four *needle variables*: the x position of the needle center (s_0), the y position of the needle center (l_0), the needle diameter (d_c), and the needle shape (a_n). The first two needle variables are referred to as the *needle position*, while the other two are referred to as the *needle geometry*.

Problem Definition: Under FCM, the needle diameter and position uniquely identify the needle path defined by the set of all \vec{P} , which is given by:

$$\vec{P} = \vec{C}_0 + \frac{d_c}{2} \hat{C}_0 P \quad (1)$$

In this equation, $\hat{C}_0 P$ is calculated at each time step.

The problem is therefore defined as finding the optimal combination of the needle variables to make a needle path that fulfills suturing guidelines.

Suture Parameters Formulation: Due to the fact that the needle variables are time-invariant during FCM, they need to be specified only once. To meet the needle grasp requirement,

we consider ST and develop the kinematic relations between the needle variables and the tissue geometry. At this instant, the suture parameters can be formulated as follows:

1) *Entry Angle:*

$$\beta_{in} = \frac{\pi}{2} + \alpha_2, 0 \leq \beta_{in} \leq \pi \quad (2)$$

TABLE I: Definition of variables in order of appearance.

Variable	Definition
C_0	Needle's geometric center
I_d	Desired needle entry point
O_d	Desired needle exit point
β_{in}	Entry angle
e_{in}	Distance between I_a and I_d
d_h	Needle depth
s_n	Needle-wound symmetry
β_{out}	Exit angle
e_{out}	Distance between O_a and O_d
s_0	x position of C_0
l_0	y position of C_0
d_c	Needle's diameter
a_n	Needle shape
P	Tip of the needle
α_2	Angle between the tissue surface and $C_0 O_a$
I_a	Actual needle entry point
G	Origin of x - y frame and midpoint of $O_d I_d$
M	Deepest point of needle
γ	Angle between $E_o O_d$ and $E_i I_d$ (tissue angle)
α_1	Angle between the tissue surface and $C_0 I_a$
O_a	Actual needle exit point
t	The distance between I_d/O_d and E_i/E_o
l_{io}	Distance between I_d and O_d
w_w	Wound width
E_i	Edge of wound on entry side
E_o	Edge of wound on exit side
Q	Rear end of the needle
h_{ti}	Input to stop unwanted needle-tissue contact
l_g	Length of the needle out of the tissue at ST
l_{ins}	Min. length of needle the instrument can grasp
λ_i	Optimization coefficients
d_t	Diameter of the trocar

2) *Distance Between Actual and Desired Needle Entry Points:*

$$e_{in} = |\overrightarrow{I_d I_a}| \quad (3)$$

3) *Needle Depth:*

$$d_h = |\overrightarrow{GM}_y - t \sin(\frac{\pi - \gamma}{2})| = |-\frac{d_c}{2} + l_0 - t \sin(\frac{\pi - \gamma}{2})| \quad (4)$$

4) *Needle-Wound Symmetry:*

$$s_n = |s_0| \quad (5)$$

5) *Exit Angle:*

$$\beta_{out} = \frac{\pi}{2} + \alpha_1, 0 \leq \beta_{out} \leq \pi \quad (6)$$

6) *Distance Between Actual and Desired Needle Exit Points:*

$$e_{out} = |\overrightarrow{O_d O_a}| \quad (7)$$

Where:

$$t = \frac{l_{io} - w_w}{2 \cos(\frac{\pi - \gamma}{2})} \quad (8)$$

For obtaining values of α_1 , α_2 , e_{in} , and e_{out} we consider the following equalities:

$$\begin{aligned} \overrightarrow{C_0 I_d} + \overrightarrow{I_d I_a} &= \overrightarrow{C_0 I_a} \\ \Rightarrow \begin{bmatrix} \frac{l_{io}}{2} - s_0 \\ 0 - l_0 \end{bmatrix} + e_{in} \hat{I}_d \hat{I}_a &= \frac{d_c}{2} C_0 \hat{I}_a \end{aligned} \quad (9)$$

$$\begin{aligned} \overrightarrow{C_0 O_d} + \overrightarrow{O_d O_a} &= \overrightarrow{C_0 O_a} \\ \Rightarrow \begin{bmatrix} -\frac{l_{io}}{2} - s_0 \\ 0 - l_0 \end{bmatrix} + e_{out} O_d \hat{O}_a &= \frac{d_c}{2} C_0 \hat{O}_a \end{aligned} \quad (10)$$

$$\begin{aligned} \det([I_d \hat{I}_a \quad I_d \hat{E}_i]) &= 0, \text{ collinear} \\ \det([O_d \hat{O}_a \quad O_d \hat{E}_o]) &= 0, \text{ collinear} \end{aligned} \quad (11)$$

$$C_0 \hat{I}_a \cdot I_d \hat{E}_i = -\cos(\alpha_2) \quad (12)$$

$$C_0 \hat{O}_a \cdot O_d \hat{E}_o = -\cos(\alpha_1)$$

Where:

$$I_d \hat{E}_i = \begin{bmatrix} \cos(\pi - (\frac{\pi - \gamma}{2})) \\ \sin(\pi - (\frac{\pi - \gamma}{2})) \end{bmatrix} \quad (13)$$

$$O_d \hat{E}_o = \begin{bmatrix} \cos(\frac{\pi - \gamma}{2}) \\ \sin(\frac{\pi - \gamma}{2}) \end{bmatrix} \quad (14)$$

(9)-(12) specify eight equations with eight unknowns of α_1 , α_2 , e_{in} , e_{out} , $I_d \hat{I}_a$, $O_d \hat{O}_a$, $C_0 \hat{I}_a$, $C_0 \hat{O}_a$. Using the solve function in MATLAB® (The MathWorks Inc., Natick, MA) and simplifying, we obtain:

$$\alpha_i = \sin^{-1}(\frac{2 \sin(\frac{\gamma}{2})}{d_c} (l_0 - \tan(\frac{\pi - \gamma}{2}) (\frac{l_{io}}{2} + (-1)^{i+1} s_0)) \quad (15)$$

$$e_{in} = \frac{-\frac{d_c}{2} \cos(\alpha_2 + \frac{\pi - \gamma}{2}) + \frac{l_{io}}{2} - s_0}{\cos(\frac{\pi - \gamma}{2})} \quad (16)$$

$$e_{out} = \frac{-\frac{d_c}{2} \cos(\alpha_1 + \frac{\pi - \gamma}{2}) + \frac{l_{io}}{2} + s_0}{\cos(\frac{\pi - \gamma}{2})} \quad (17)$$

Note that β_{in} , β_{out} , e_{in} , and e_{out} are nonlinear functions of the needle variables.

Ideal Suture Parameters: Based on the suturing guidelines, it is possible to quantify ideal values for each suture parameter. The ideal β_{in} and β_{out} are $\frac{\pi}{2}$. e_{in} , e_{out} , and s_n should each be zero. d_h is usually set to $\frac{l_{io}}{2}$, but can be changed if the surgeon prefers a different needle depth.

Kinematic Constraints: The kinematic constraints between the needle and tissue are defined at BT, ST, and ET. To keep our analysis general, kinematics constraints imposed by the robot such as RCM are not considered.

1) *Bite time constraint:*

$$\overrightarrow{Q}_y - t \sin(\frac{\pi - \gamma}{2}) \geq h_{ti} \quad (18)$$

Where:

$$\begin{bmatrix} \overrightarrow{Q}_x \\ \overrightarrow{Q}_y \end{bmatrix} = \begin{bmatrix} \cos(2\pi a_n) & -\sin(2\pi a_n) \\ \sin(2\pi a_n) & \cos(2\pi a_n) \end{bmatrix} \overrightarrow{C_0 I_a} + \begin{bmatrix} s_0 \\ l_0 \end{bmatrix} \quad (19)$$

$$\overrightarrow{C_0 I_a} = \begin{bmatrix} \frac{w_w}{2} + (t - e_{in}) \cos(\frac{\pi - \gamma}{2}) - s_0 \\ e_{in} \sin(\frac{\pi - \gamma}{2}) - l_0 \end{bmatrix} \quad (20)$$

Equation (18) states that Q must be at least h_{ti} (an input) above the surface of the tissue.

2) *Switching time constraints:*

$$l_g \geq l_{ins} \quad (21)$$

$$|\overrightarrow{I_a O_a}| \geq w_w \quad (22)$$

$$\overrightarrow{GM}_y - t \sin(\frac{\pi - \gamma}{2}) \leq 0 \quad (23)$$

$$\begin{aligned} \frac{\overrightarrow{I_d I_a} \cdot \overrightarrow{I_d E_i}}{t^2} &\leq 1 \\ \frac{\overrightarrow{O_d O_a} \cdot \overrightarrow{O_d E_o}}{t^2} &\leq 1 \end{aligned} \quad (24)$$

Where:

$$l_g = \frac{\pi a_n d_c - \frac{d_c}{2} (\gamma - \alpha_1 - \alpha_2)}{2} \quad (25)$$

$$|\overrightarrow{I_a O_a}| = d_c \sin(\frac{\gamma - \alpha_1 - \alpha_2}{2}) \quad (26)$$

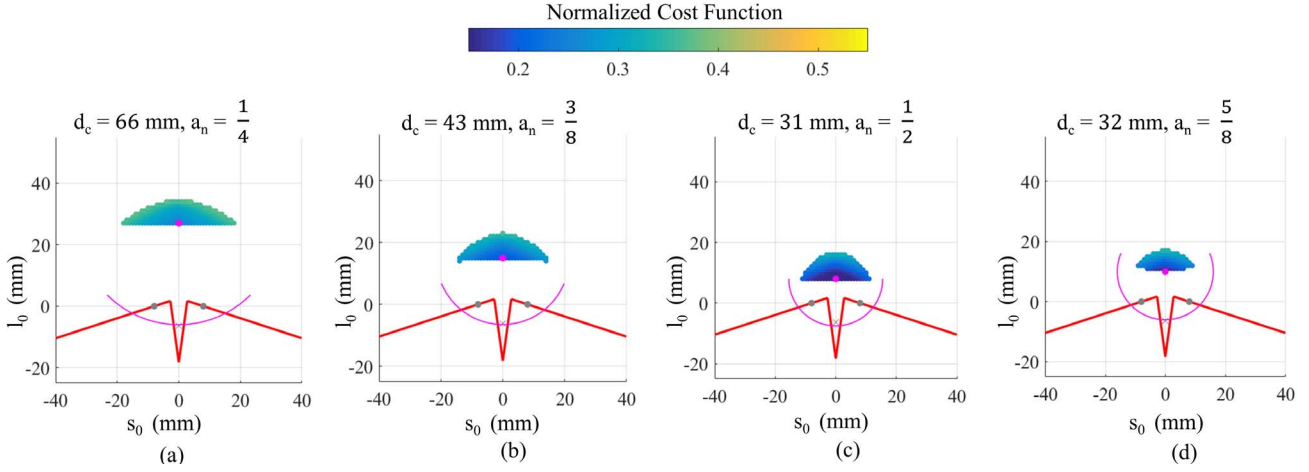


Fig. 5: Optimal 2D Feasible Solution Subsets for (a) $d_c = 66$ mm and $a_n = \frac{1}{4}$, (b) $d_c = 43$ mm and $a_n = \frac{3}{8}$, (c) $d_c = 31$ mm and $a_n = \frac{1}{2}$, (d) $d_c = 32$ mm and $a_n = \frac{5}{8}$.

and equal contribution (16.6%) of suture parameters to the solution. In order to show the full 4D feasible solution set, the 3D feasible solution subset for each a_n is plotted with the calculated normalized cost of each point. Note that standard suture needles do not exceed 77 mm in diameter [26], providing the upper bound on each of the subplots.

B. Optimal 2D Feasible Solution Subsets

Fig. 5 displays the 2D feasible solution subsets with optimal d_c for each a_n . The normalized cost of each point is displayed. The pink points are the optimal s_0 and l_0 for each of the 2D feasible solution subsets. The pink curves show the needles centered at the optimal s_0 and l_0 at ST.

C. Effects of Optimization Weighting Factors

$\lambda_i s$ are optimization weighting factors which are selected based on the recommendations of the surgeon. Fig. 7 depicts results of simulations with the same input set previously listed, but with different optimization weighting factors.

D. Effects of Tissue Geometry

To demonstrate the effects of tissue geometry on optimal needle variables, different sets of γ and w_w were simulated and the results are presented in Table II. l_{io} was set to three times w_w for each scenario. All other input variables were kept the same as in Fig. 4.

TABLE II: Optimal needle variables for different tissue geometries.

γ	w_w	Opt. d_c	Opt. a_n	Opt. l_0	Opt. s_0
π	1 mm	27 mm	$\frac{1}{2}$	9 mm	0 mm
π	5 mm	36 mm	$\frac{3}{4}$	10 mm	0 mm
$\frac{\pi}{6}$	1 mm	15 mm	$\frac{1}{2}$	7 mm	0 mm
$\frac{\pi}{8}$	5 mm	58 mm	all	28 mm	0 mm
$\frac{3\pi}{4}$	1 mm	26 mm	$\frac{1}{2}$	1 mm	0 mm
$\frac{3\pi}{4}$	5 mm	53 mm	$\frac{3}{4}$	17 mm	0 mm

IV. ROBOTIC EXPERIMENTAL VERIFICATION:

A. Experiment Setup

To experimentally evaluate the proposed algorithm, a Raven II surgical robotic system was used. The system consists of multiple three-degree-of-freedom (3-DOF) cable-actuated spherical positioning mechanisms designed for use with interchangeable 4-DOF instruments. A single manipulator of the Raven II, outfitted with a large needle driver (Intuitive Surgical, Inc.), was deployed. Similar to [14], a 3D-printed jaw-mounted needle guide (see Fig. 6) was utilized to enable the needle driver to securely grasp the suturing needle. The suturing is completed on a ITM-30 tissue phantom from Simulab Corp. The phantom was manipulated to modify tissue angle (see Fig. 1). Based on the results of the simulation (see Fig. 5c), a size 1 CTX taper point needle (Ethicon Inc.) with $a_n = \frac{1}{2}$ and $d_c = 30.55$ mm was used.

B. Experiment Results

The robot was programmed to complete a CCP from BT to ST. A complete sequence of the needle motion is shown in Fig. 6. Eight trials of automated suturing were performed. Direct measurements were obtained for e_{in} , e_{out} , and d_h . Geometric relations of the measured distances between Q , I_a , and E_i , as well as P , O_a , and E_o were used to obtain β_{in} and β_{out} respectively. The calculated β_{in} and β_{out} along with the measured $E_o E_i$ were used to acquire s_n . Each

TABLE III: Desired, simulation, and experiment suture parameter values.

Suture Param.	Desired	Simulation	Experiment
β_{in}	1.57 rad	1.91 rad	1.96 ± 0.07 rad
e_{in}	0 mm	4.56 mm	4.83 ± 0.62 mm
d_h	7.99 mm	9.15 mm	8.44 ± 0.73 mm
s_n	0 mm	0 mm	0.25 ± 0.12 mm
β_{out}	1.57 rad	1.91 rad	2.03 ± 0.11 rad
e_{out}	0 mm	4.56 mm	4.69 ± 0.57 mm

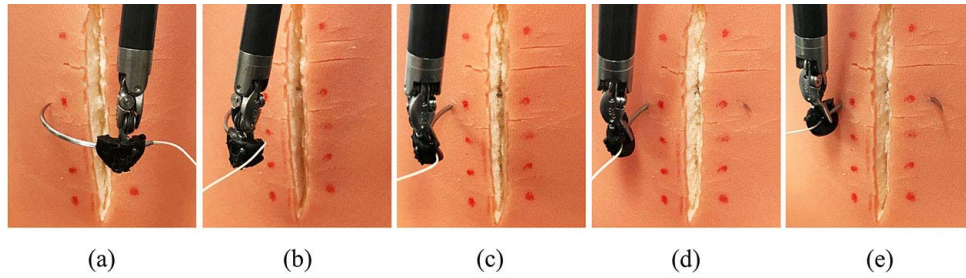


Fig. 6: Sequential images of automated suturing experiment from bite time (a) to switching time (e).

measurement was taken three times. The mean and standard deviation of each suture parameter is given in Table III.

V. DISCUSSION

A. Feasible Solution Set

The feasible solution set produced by the algorithm, shown in Fig. 4 and Fig. 5, can be examined for accuracy. Physically, a larger diameter allows the needle to translate further in both x- and y-directions while maintaining a valid configuration. Minimum l_0 is dictated by needle diameter and shape due to the grasp constraint. Additionally, the BT and ET constraints disallow solutions with large a_n , small l_0 , and large $|s_0|$ as is particularly noticeable for $a_n = \frac{\pi}{6}$. Without the BT and ET constraints, the 3D subsets of larger shapes would fully contain the 3D subsets of all smaller shapes.

B. Cost

Each point displayed in Fig. 4 and Fig. 5 is color coded based on the calculated cost, with dark blue corresponding to lowest cost and bright yellow to highest cost. It should be noted that although the validity of any particular solution is in part determined by needle shape, the cost is not dependent on needle shape. For the given input set, in which all suture parameters contribute evenly, the algorithm heavily favors solutions with small $|s_0|$ as this creates symmetry.

C. Optimization Weighting Factors

In Fig. 7, each needle solution closely satisfies the parameters for which it is heavily weighted. It should be noted that not all of the input sets of λ_i are clinically realistic, but are chosen to demonstrate the performance of the algorithm. The solution in (i) overwhelmingly favors β_{in} and d_h , and therefore performs poorly in terms of the other parameters (most notably e_{in}). The solution in (iii) results in a very large d_c to satisfy (21) while almost only considering β_{in} and β_{out} . Note that when β_{in} and/or β_{out} are heavily favored, the needle center tends towards the line of the tissue surface (case (i), (iii), and (iv)).

D. Effects of Tissue Geometry

As previously mentioned, surgeons select suturing needles based on tissue geometry. Table II shows that our model

captures this by outputting different optimal needle variables. Our model suggests that there is no practical difference between needle shapes, when all other variables are optimal, in some suturing situations (e.g. $\gamma = \frac{\pi}{6}$ and $w_w = 5$ mm).

E. Error Sources in the Experiment

Table III shows that the experimental results very closely match the simulation results despite several sources of error. These sources include:

Tissue Geometry Approximation: The algorithm assumes the tissue does not curve on either side of the wound. The manipulated tissue phantom had a concave down surface. As such, the measured d_h was less than simulated. Furthermore, all points on the tissue move slightly during each trial due to needle-tissue interaction forces [22].

Flexibility in the Robot: Compliance in the Raven II and the large needle driver cause error between the programmed and actual paths of the tool tip. This can lead to unmodeled forces/torques between the tissue and the needle [27].

Deformation and Deflection of the Needle: While the algorithm assumes tissue with negligible resistance, the actual tissue does provide resistive forces/torques to motion even with an ideal CCP. Additionally, even with the needle guide, some deflection can occur between needle and tool tip.

F. Application to MIS

The algorithm is generic and applicable to both MIS and open surgery. The values of l_{ins} and h_{ti} in the experimental setup were chosen due to use of an 8 mm wide jaw-mounted needle guide. This limited the solution set to relatively large needle diameters appropriate for open surgery. In clinical MIS applications these values could be reduced to 2-3 mm each. This could permit needles with small enough diameters to fit through the trocar. In particular, the results of the algorithm with identical inputs to the previous simulation (Fig. 4) but with $l_{ins} = h_{ti} = 3$ mm will be $s_0 = 0$ mm, $l_0 = 3$ mm, $a_n = \frac{1}{2}$, $d_c = 18$ mm which can fit in a 10 mm trocar. For MIS applications, the following inequality which provides a reduced upper bound for d_c , based on trocar diameter (d_t), should be added to the algorithm:

$$d_c \leq \csc^2\left(\frac{a_n\pi}{2}\right)d_t \quad (30)$$

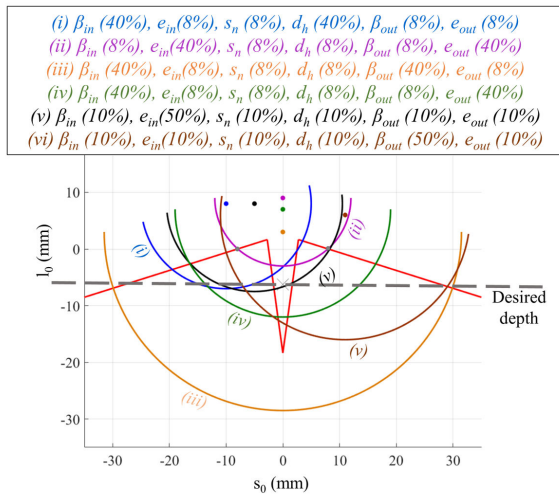


Fig. 7: Simulations for various optimization weighting factors

VI. CONCLUSION

In this paper, we presented a constant curvature path planning algorithm which minimizes tissue trauma and optimizes needle variables to satisfy recommended suturing guidelines. The main novelty of our method is to allow and minimize errors for all the suture parameters rather than satisfying just a few, as was considered in previous studies.

The algorithm correctly identifies the feasible solution set, calculates the cost of each solution, and selects the lowest cost solution for any input set. The output was examined for numerous situations with variations in tissue geometry and optimization weighting factors.

The accuracy of the model was tested on a tissue phantom using the Raven II. The measured results indicate the model is accurate and the assumptions are reasonable.

REFERENCES

- [1] A. Garcia-Ruiz, M. Gagner, J. H. Miller, C. P. Steiner, and J. F. Hahn, "Manual vs robotically assisted laparoscopic surgery in the performance of basic manipulation and suturing tasks," *Archives of surgery*, vol. 133, no. 9, pp. 957–961, 1998.
- [2] J. Rosen, B. Hannaford, and R. M. Satava, *Surgical robotics: systems applications and visions*. Springer Science & Business Media, 2011.
- [3] B. Hannaford, J. Rosen, D. W. Friedman, H. King, P. Roan, L. Cheng, D. Glozman, J. Ma, S. N. Kosari, and L. White, "Raven-ii: an open platform for surgical robotics research," *IEEE Transactions on Biomedical Engineering*, vol. 60, no. 4, pp. 954–959, 2013.
- [4] O. Jacob Isaac-Lowry, S. Okamoto, S. A. Pedram, R. Woo, and P. Berkelman, "Compact teleoperated laparoendoscopic single-site robotic surgical system: Kinematics, control, and operation," *The International Journal of Medical Robotics and Computer Assisted Surgery*, In Press, 2017.
- [5] J. Ruurda, I. Broeders, B. Pulles, F. Kappelhof, and C. Van der Werken, "Manual robot assisted endoscopic suturing: time-action analysis in an experimental model," *Surgical endoscopy and other interventional techniques*, vol. 18, no. 8, pp. 1249–1252, 2004.
- [6] A. Knoll, H. Mayer, C. Staub, and R. Bauernschmitt, "Selective automation and skill transfer in medical robotics: a demonstration on surgical knot-tying," *The International Journal of Medical Robotics and Computer Assisted Surgery*, vol. 8, no. 4, pp. 384–397, 2012.
- [7] J. Van Den Berg, S. Miller, D. Duckworth, H. Hu, A. Wan, X.-Y. Fu, K. Goldberg, and P. Abbeel, "Superhuman performance of surgical tasks by robots using iterative learning from human-guided demonstrations," in *Proc. of IEEE International Conference on Robotics and Automation (ICRA)*, 2010, pp. 2074–2081.
- [8] H. Kang and J. T. Wen, "Autonomous suturing using minimally invasive surgical robots," in *Proc. of the International Conference on Control Applications*, 2000, pp. 742–747.
- [9] N. Padoy and G. D. Hager, "3d thread tracking for robotic assistance in tele-surgery," in *Proc. of IEEE/RSJ International Conference on Intelligent Robots and Systems*, 2011, pp. 2102–2107.
- [10] S. Javdani, S. Tandon, J. Tang, J. F. O'Brien, and P. Abbeel, "Modeling and perception of deformable one-dimensional objects," in *IEEE Int'l Conf. on Robotics and Automation (ICRA)*, 2011, pp. 1607–1614.
- [11] T. Liu and M. C. Cavusoglu, "Needle grasp and entry port selection for automatic execution of suturing tasks in robotic minimally invasive surgery," *IEEE Transactions on Automation Science and Engineering*, vol. 13, no. 2, pp. 552–563, 2016.
- [12] T. Liu and M. C. Çavuşoğlu, "Optimal needle grasp selection for automatic execution of suturing tasks in robotic minimally invasive surgery," in *Proc. of IEEE International Conference on Robotics and Automation (ICRA)*, 2015, pp. 2894–2900.
- [13] F. Nageotte, P. Zanne, C. Doignon, and M. De Mathelin, "Stitching planning in laparoscopic surgery: Towards robot-assisted suturing," *Int'l Journal of Robotics Research*, vol. 28, no. 10, pp. 1303–1321, 2009.
- [14] S. Sen, A. Garg, D. Gealy, S. McKinley, Y. Jen, and K. Goldberg, "Automating multi-throw multilateral surgical suturing with a mechanical needle guide and sequential convex optimization," in *IEEE International Conference on Robotics and Automation (ICRA)*, 2016.
- [15] S. Iyer, T. Looi, and J. Drake, "A single arm, single camera system for automated suturing," in *Proceedings of IEEE International Conference on Robotics and Automation (ICRA)*, pp. 239–244, 2013.
- [16] C. Staub, T. Osa, A. Knoll, and R. Bauernschmitt, "Automation of tissue piercing using circular needles and vision guidance for computer aided laparoscopic surgery," in *Proc. of IEEE International Conference on Robotics and Automation (ICRA)*, pp. 4585–4590, 2010.
- [17] E. Diao, J. S. Hariharan, O. Soejima, and J. C. Lotz, "Effect of peripheral suture depth on strength of tendon repairs," *The Journal of hand surgery*, vol. 21, no. 2, pp. 234–239, 1996.
- [18] T. J. Zimmerman, T. Krupin, W. Grodzki, and S. R. Waltman, "The effect of suture depth on outflow facility in penetrating keratoplasty," *Archives of ophthalmology*, vol. 96, no. 3, pp. 505–506, 1978.
- [19] R. C. Jackson and M. C. Cavusoglu, "Needle path planning for autonomous robotic surgical suturing," in *Proc. of IEEE Int'l Conference on Robotics and Automation (ICRA)*, pp. 1669–1675, 2013.
- [20] J. Ding and N. Simaan, "Choice of handedness and automated suturing for anthropomorphic dual-arm surgical robots," *Robotica*, vol. 33, no. 08, pp. 1775–1793, 2015.
- [21] A. Kapoor, M. Li, and R. H. Taylor, "Spatial motion constraints for robot assisted suturing using virtual fixtures," in *Medical Image Computing and Computer-Assisted Intervention (MICCAI)*, pp. 89–96, 2005.
- [22] F. H. Khabbaz and A. Patriciu, "Stitching path planning using circular needles-tissue interaction model," in *IEEE International Conference on Robotics and Biomimetics (ROBIO)*, 2011, pp. 1134–1139.
- [23] J. Hochberg, K. M. Meyer, and M. D. Marion, "Suture choice and other methods of skin closure," *Surgical Clinics of North America*, vol. 89, no. 3, pp. 627–641, 2009.
- [24] R. Edlich, R. R. Szarmach, J. Livingston, G. T. Rodeheaver, and J. G. Thacker, "An innovative surgical suture and needle evaluation and selection program," *Journal of long-term effects of medical implants*, vol. 12, no. 4, 2002.
- [25] D. A. Sherris and E. B. Kern, *Essential surgical skills*. WB Saunders Company, 2004.
- [26] Ethicon Inc., <http://woundclosure.ethicon.com/>.
- [27] R. C. Jackson and M. C. Çavuşoğlu, "Modeling of needle-tissue interaction forces during surgical suturing," in *Proc. of 2012 IEEE International Conference on Robotics and Automation (ICRA)*, 2012, pp. 4675–4680.